Synthesis, DFT Calculations, DNA Interaction, and Antimicrobial Studies of Some Mixed Ligand Complexes of Oxalic Acid and Schiff Base Trimethoprim with Various Metal Ions

Eid Abdalrazaq[1*], Abdel Aziz Qasem Jbarah[1], Tagreed Hashim Al-Noor[2], Gassan Thabit Shinain[2], and Mohammed Mahdi Jawad[3]

[1]*Department of Chemistry, College of Science, Al-Hussein Bin Talal University, Ma'an 71111, Jordan*

[2]*Department of Chemistry, Education for Pure Science College - Ibn- Al Haitham, University of Baghdad, Baghdad 10071, Iraq*

[3]*Department of Biology, Education College - Ibn- Al Haitham, University of Baghdad, Baghdad 10071, Iraq*

Corresponding author:

tel: +962-796862267
email: eidalzooby@yahoo.com

Received: April 9, 2022
Accepted: July 19, 2022

DOI: 10.22146/ijc.74020

Abstract: *Mixed ligand metal complexes are synthesized from oxalic acid with Schiff base, and the Schiff base was obtained from trimethoprim and acetylacetone. The synthesized complexes were of the type [**M**(**L**$_1$)(**L**$_2$)], where the metal, **M**, is Ni(II), Cu(II), Cr(III), and Zn(II), **L**$_1$ corresponds to the trimethoprim ((Z)-4-((4-amino-5-(3,4,5-trimethoxybenzyl)pyrimidine-2-yl)imino)pentane-2-one) as the first ligand and **L**$_2$ represent the oxalate anion ($C_2O_2^{2-}$) as a second ligand. Characterization of the prepared compounds was performed by elemental analysis, molar conductivity, magnetic measurements, ^{1}H-NMR, ^{13}C-NMR, FT-IR, and Ultraviolet-visible (UV-Vis) spectral studies. The recorded infrared data is reinforced with density functional theory (DFT) calculations. Also, the recorded and calculated IR spectra of the complexes suggested that the coordination of Schiff base is a bidentate ligand with Cu and Ni complexes and a tridentate ligand with Co, Cr, and Zn complexes. The electronic structures of the complexes were investigated by DFT calculations, showing several degrees of HOMO-LUMO energy gaps between complexes. The complexes were studied for their DNA interaction activities. The synthesized ligand and its metal complexes were evaluated for antimicrobial properties against bacterial strains of* Bacillus subtilis *(G+),* Enterobacter cloacae *(G-), and* Staphylococcus aureus *(G+). These complexes considered in this study showed good antimicrobial activity.*

Keywords: *trimethoprim; oxalic acid complexes; acetyl acetone; Schiff base; antimicrobial activity*

■ INTRODUCTION

Schiff base compounds showed a unique role as ligands with transition metals and main groups in bioinorganic and coordination chemistry [1-2]. The interaction of Schiff bases with metal ions gives complexes of different geometries used as anticancer, antibacterial, antiviral, design medicinal compounds, antitumor organometallic chemistry, catalytic applications, chemical analysis, geology, and corrosion inhibition [3-4]. The complexes with mixed ligands of a Schiff base 4-dihydroxybenzylidenethiosemicarbazide (H_2L)-, Oxalic Acid and with, M(II) = Cu, Zn, Ni and Fe(III) ions [5]. The H_2L is coordinated to the metal atom as a neutral, monoanionic, or dianionic tetradentate type (ONNO) ligand in its complexes. Chen [6] has reported the synthesis and structural characterization of a trans-$(PyH)_2[Mo_2O_4(C_2O_4)_2(Py)_2]$ in an aqueous solution. The pyridine ligand coordinates to the Mo atom through the N atom. The oxalate ligand coordinates to each Mo atom through 2-Carboxylate Oxygen atoms in a bidentate chelating manner. Based on these observations, the present study was undertaken to synthesize and

characterize mixed ligand complexes of oxalate anion and Schiff base derived from trimethoprim and acetylacetone with one of the metal ions Cr(III), Co(II), Ni(II), Cu(II) and Zn(II). DFT calculations for molecular electrostatic potential, geometry optimization and vibrational frequencies of the synthesized molecules using the B3LYP level of theory and LANL2DZ basis set were reported.

■ EXPERIMENTAL SECTION

Materials

All the chemicals and solvents, trimethoprim, ethanol, acetylacetone, acetic acid, dimethyl sulfoxide, chloroform, methanol, and acetone metal chloride salts, were purchased of A.R. Grade quality obtained from Aldrich, Merck, and BDH and were used without further purification.

Instrumentation

Melting points were determined by MPA160 – Digi Melt melting point instrument. The Eager300 obtained the Elemental analysis of ligand for EA1112 Thermal Finnegan C.H.N.S 2400 instrument. The atomic absorption spectrophotometer analysis of the complexes was measured using a fair agreement method using the device from type Shimadzu (A.A 620) atomic absorption spectrophotometer. The molar conductivity values of the complexes with a concentration of 10^{-3} mol/L in dimethyl sulfoxide (DMSO) were reached by the digital conductivity series Ino.Lab.720 device. The Magnetic susceptibility measurements of the complexes were measured using Johnson Mattey Balance. Ultraviolet-visible spectra were recorded on double-beam UV-Visible spectrophotometry of the type U.V 160A (Shimadzu) at 200 and 1100 nm with a 1 cm quartz cell, using DMSO as a solvent and a concentration of 10^{-3} mol/L. The Fourier-transform infrared spectra were measured using KBr pellets on the Shimadzu FTIR 8400S spectrophotometry instrument. The spectra FTIR are recorded in the range of 400 to 4000 cm^{-1}. The ^{1}H and ^{13}C-NMR spectra were obtained from the DMSO-d_6 solution using an Inova 500 MHz instrument.

Procedure

Synthesis of Schiff base ligand

The Schiff base ligand ($\mathbf{L_1}$) was prepared by condensation of 1.176 g (4 mmol) of trimethoprim in 20 mL ethanol and 0.4 g (4 mmol) acetylacetone for 8 h with the addition of 4 to 5 drops of acetic acid (Scheme 1). The volume of the mixture was reduced by slow evaporation at room temperature and leave it to stand overnight. Then, the obtained off-white precipitate was washed several times with absolute ethanol, dried at room temperature, and recrystallized from ethanol to get a pure sample.

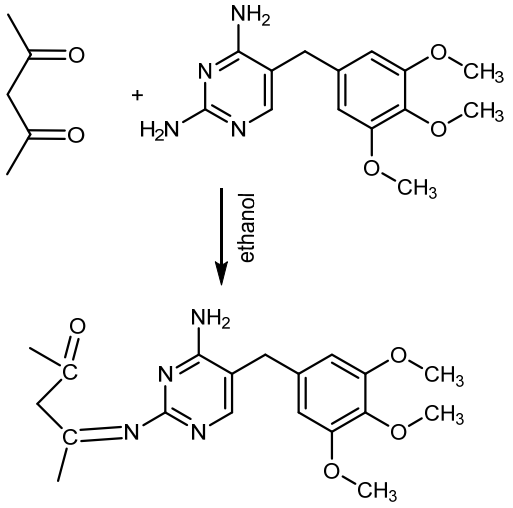

(*Z*)-4-((4-amino-5-(3,4,5-trimethoxybenzyl)pyrimidin-2-yl)imino)pentan-2-one

Scheme 1. The synthesis route of Schiff base ligand, $\mathbf{L_1}$

$C_{19}H_{24}N_4O_4$ (**L_1**): %Yield: 86%. Anal. calc. for $C_{19}H_{24}N_4O_4$ (372.43 g/mol): C, 61.27; H, 6.50; N, 15.05. Found C, 62.06; H, 5.56; N, 13.99. Mp: 185 °C. IR (KBr, cm^{-1}): ν(C=O) 1682, ν(−C=N−) 1658. ^{1}H-NMR (DMSO-d_6): δ 1.880 (-N=C-C**H**$_3$), 2.490 ((CO)-C**H**$_3$), 3.518–3.605 (C**H**$_2$), 3.710 (O-C**H**$_3$), 5.966 (pyrimidine ring), 6.545–6.252 (N**H**$_2$), 7.487 (Ar). ^{13}C-NMR (500 MHz, DMSO-d_6): δ 18.5 (-N=C-**C**H$_3$), 21.3 (-(CO)-**C**H$_3$). 55.8 (O-**C**H$_3$), 59.9 (**C**H$_2$), 105.6–135.8 (Ar), 152.7–161.6 (pyrimidine ring), 162.3 (-**C**=N), 172.5 (**C**=O).

Synthesis of the complexes of the type [M(L_1)(L_2)]

The complexes were prepared in a molar ratio of 1:1:1 (**M**:**L_1**:**L_2**). The metal chloride salts ($MCl_2{\cdot}nH_2O$. n = 0–6, and $CrCl_3{\cdot}6H_2O$) reacted with the two ligands according to Scheme 2 and the following proposed general equation:

$H_2C_2O_4 + 2KOH \rightarrow K_2C_2O_4 + 2H_2O$

M$Cl_2{\cdot}nH_2O$ + **L_1** + K_2**L_2** → [**M**(**L_1**)(**L_2**)] + 2KCl + nH_2O

where **L_1** = Schiff base (the first ligand), **L_2** = $C_2O_4^{2-}$ (Oxalate anion as a second ligand) and **M** = the corresponding metal.

Dissolving 0.23793, 0.23769, 0.17048, 0.17228 and 0.26635 g (1 mmol) of $CoCl_2{\cdot}6H_2O$, $NiCl_2{\cdot}6H_2O$, $CuCl_2{\cdot}2H_2O$, $ZnCl_2$, and $CrCl_3{\cdot}6H_2O$, respectively, in 10 mL of ethanol. A 0.372 g (1 mmol) of **L_1** in 10 mL of ethanol and the solution of potassium oxalate were added at the same time to the metal chloride solution. The mixture was stirred for 4 h at room temperature and left for 24 h. The precipitate was filtered and washed with ethanol before recrystallizing and drying at room temperature. The percentage yield range is 79 to 85%.

$CoC_{21}H_{24}N_4O_8$ (**1**): %Yield: 83%. Anal. calc. for $CoC_{21}H_{24}N_4O_8$ (519.38 g/mol): C, 48.56; H, 4.66; N, 10.79. Found C, 49.02; H, 4.44; N, 11.13. Mp: 223–255 °C. IR (KBr, cm^{-1}): ν(C=O) 1670 (carbonyl of **L_1**), ν(−C=N−) 1645, ν(C-O) 1238 (oxalate), ν(Co-N) 524, ν(Co-O) 480 (oxygen of **L_2**), ν(Co-O) 459 (oxygen of **L_1**).

$CrC_{21}H_{24}N_4O_8$ (**2**): %Yield: 82%. Anal. calc. for $CrC_{21}H_{24}N_4O_8$ (512.44 g/mol): C, 49.22; H, 4.72; N, 10.93. Found C, 48.78; H, 4.36; N, 10.61. Mp: 285 °C. IR (KBr, cm^{-1}): ν(C=O) 1671 (carbonyl of **L_1**), ν(−C=N−) 1643, ν(C-O) 1235 (oxalate), ν(Cr-N) 526, ν(Cr-O) 475 (oxygen of **L_2**), ν(Cr-O) 448 (oxygen of **L_1**).

$ZnC_{21}H_{24}N_4O_8$ (**3**): %Yield: 79%. Anal. calc. for $ZnC_{21}H_{24}N_4O_8$ (525.82 g/mol): C, 47.97; H, 4.60; N, 10.66. Found C, 48.11; H, 4.98; N, 10.85. Mp: 216–220 °C. IR (KBr, cm^{-1}): ν(C=O) 1674 (carbonyl of **L_1**), ν(−C=N−) 1643, ν(C-O) 1242 (oxalate), ν(Zn-N) 542, ν(Zn-O) 484 (oxygen of **L_2**), ν(Zn-O) 438 (oxygen of **L_1**).

$CuC_{21}H_{24}N_4O_8$ (**4**): %Yield: 83%. Anal. calc. for $CuC_{21}H_{24}N_4O_8$ (523.99 g/mol): C, 48.14; H, 4.62; N, 10.69. Found C, 49.03; H, 4.86; N, 10.93. Mp: 253–255 °C. IR (KBr, cm^{-1}): ν(C=O) 1681 (carbonyl of **L_1**), ν(−C=N−) 1642, ν(C-O) 1240 (oxalate), ν(Cu-N) 513, ν(Cu-O) 479 (oxygen of **L_2**).

$NiC_{21}H_{24}N_4O_8$ (**5**): %Yield: 85%. Anal. calc. for $NiC_{21}H_{24}N_4O_8$ (519.14 g/mol): C, 48.59; H, 4.66; N, 10.79. Found C, 47.82; H, 4.92; N, 10.41. Mp: 216 °C. IR (KBr, cm^{-1}): ν(C=O) 1680 (carbonyl of **L_1**), ν(−C=N−) 1643, ν(C-O) 1245 (oxalate), ν(Ni-N) 532, ν(Ni-O) 472 (oxygen of **L_2**).

DNA binding properties

DNA was extracted from human blood samples without any health problems in the city of Baghdad/Iraq

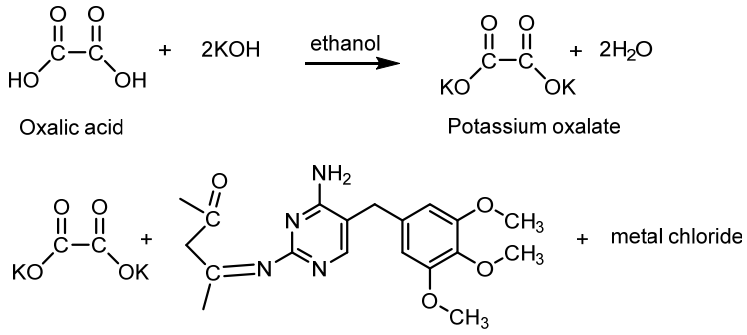

Scheme 2. The synthesis route of the complexes contains Schiff base ligand and metal ion

using unique extraction from Promiga USA. The steps mentioned in the protocol were followed. The DNA concentration and the purity of the extracted DNA were obtained using the spectrophotometer of 1.6 to 1.8 ng/mL. The purity and concentration were measured using the subject standards. The samples were initially extracted on the 1% agarose gel to confirm their quality and to see if there was any breakage during extraction. The studied materials were then mixed with the extracted DNA by 2:1 v/v and put in a water bath for one hour at 37 °C and then transported in 1.5% agarose gel for 1 h and 75 V, then treated with Red safe fluorescent dye and under the UV source using the gel documentation system.

Computational details

All the DFT calculations were performed with the Gaussian09 program [7]. The geometries of the complexes were fully optimized at B3LYP (Becke's, three-parameter exchange functional, in combination with Lee-Yang-Parr correlation function) [8-10] with the 6-311G* basis set for C, H, O and N atoms and LANL2DZ (Los Alamos National Laboratory 2 double-zeta) [11-13] basis set for metal atom. LANL2DZ is an effective core potential (ECP) type and has been widely used for studies of transition metals (TM) containing systems. The computational cost is decreased with the chemically inactive core electrons represented by an ECP since the cost formally increases as ~N4, where N is the number of explicitly treated electrons. The program GaussView 6 [14] was used to inspect the input and output files generated by Gaussian09 for pre-processing, structure modification, and post-processing analyses of structures, frequencies, and forces. A frequency analysis was performed for each stationary point to identify the minima's most stable structure. All minima have no imaginary frequencies in the vibrational mode calculations. The molecular electrostatic potential, V(r), at a given point r(x,y,z) in the vicinity of a molecule, to determine the reactive sites of the complexes, was calculated at the B3LYP functional with the 6-311G* basis set for C, H, O and N atoms and LANL2DZ basis set for the metal atom of the optimized geometry. The definition, description, and calculation of V(r) were reported in many reports [15]. The B3LYP level of theory with the 6-311G* basis set for C, H, O, and N atoms and the LANL2DZ basis set for metal atoms is used to calculate the energies and electron densities of the frontiers molecular orbitals. The PDOS (Projected density of states) has been obtained via the calculated orbital populations for all synthesized complexes at the same level of theory, using GAUSSSUM 3.0 program [16].

■ RESULTS AND DISCUSSION

The solubility of the compounds was tested using various solvents. The synthesized complexes are non-hygroscopic solids, varying colors and soluble in water and dimethyl sulfoxide, whereas insoluble in ethanol, chloroform, methanol, and acetone. Also, they are air-stable at room temperature. The molecular weight, melting point, and Flame-AAS analysis of the synthesized complexes were carried out by the literature methods [17]. The experimental and calculated values of a metal content percent (M%) in all complexes are in fair agreement. The chloride ions test in all complexes was done with the $AgNO_3$ solution, and a negative result was obtained [18]. The molar conductance values of the complexes in DMSO solvent indicated that $[ML_1L_2]$ complexes are non-electrolytes, while complex **2** is a 1:1 electrolyte [19-20]. These results support the proposed formula of the complexes (Fig. 1). The physical and analytical data of Schiff base ligand $\mathbf{L_1}$, and its metal complexes are listed in Table 1.

^{1}H-NMR Result

The ^{1}H-NMR in the DMSO-d_6 solvent of the ligand ($\mathbf{L_1}$) is shown in S1. In S1, two signals appeared at 3.605 and 3.518 ppm, which were assigned to the protons of the CH_2 groups. The previously reported values of the CH_2 group signals in the ^{1}H-NMR spectrum are in the range of 3.59–3.52 ppm [20]. The spectrum of the ligand, S1, also showed a peak at 3.710 ppm. This peak is attributed to the methoxy protons (O-CH_3 group). The chemical shifts of the protons of the O-CH_3 group are reported in the range of 3.65–3.8 ppm [21-23]. The chemical shift of the benzene ring protons is found at 7.487 ppm. It was reported that the chemical shift of the

Table 1. Analytical data and some physical measurements of the Schiff base ligand and the complexes

Compound	Molecular weight (g/mol)	Color	Melting point (°C)	M%	Molar conductance Λ ($\Omega^{-1}cm^2mol^{-1}$)
$\mathbf{L_1}$	372.43	Yellow	185	-	-
1	519.38	Pink	223–255	11.35[a]	25.88[c]
				10.85[b]	
2	512.44	Dark green	285	10.15[a]	37.88[c]
				10.20[b]	
3	525.82	White	216–220	12.43[a]	17.18[c]
				11.93[b]	
4	523.99	Off white	253–255	12.13[a]	16.55[c]
				11.13[b]	
5	519.14	Light green	216	11.31[a]	18.6[c]
				10.20[b]	

[a]: theoretical value, [b]: experimental value, [c]: measured in DMSO

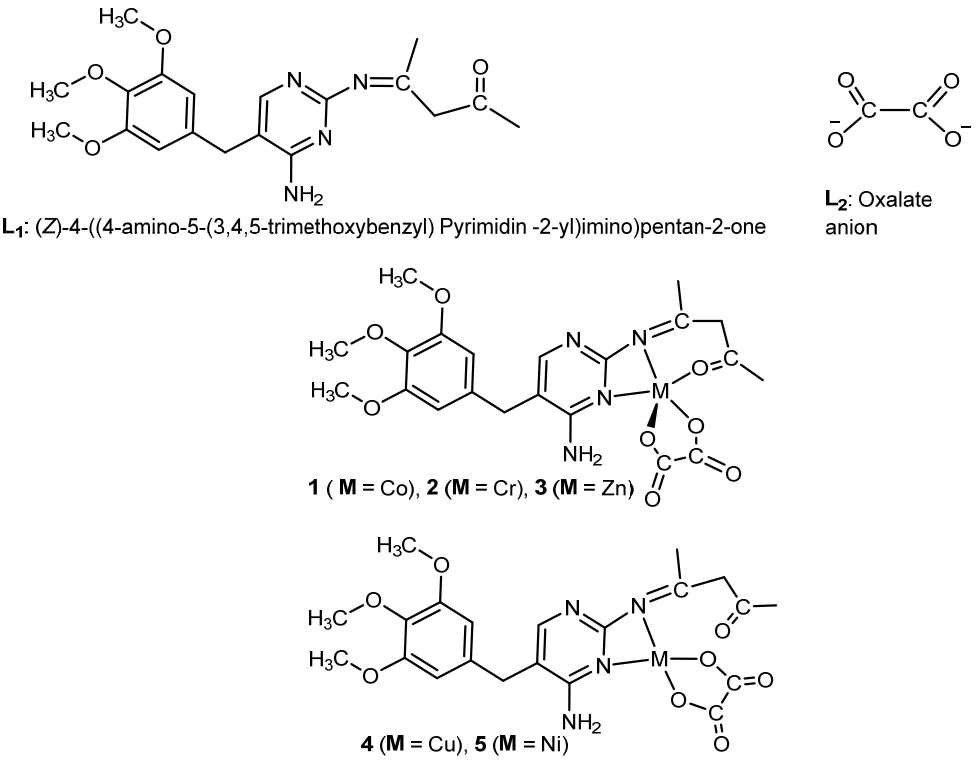

Fig 1. The suggested structure of the complexes [$\mathbf{M(L_1)(L_2)}$]) and ligands

benzene ring protons displayed in 6.75–8.01 ppm [23-24]. The chemical shift of the proton of the pyrimidine ring is observed at 5.966 ppm. The protons of the amine group (NH_2) showed two peaks at 6.545 and 6.252 ppm. The reported values for the pyrimidine ring proton and the protons of the amine group are 5.8 and 6.9, respectively [25]. The chemical shifts of the methyl protons of the (-N=C-C$\underline{\mathbf{H}}_3$) and ((CO)-C$\underline{\mathbf{H}}_3$) groups were observed at 1.880 and 2.490 ppm, respectively [26].

^{13}C-NMR Results

The ^{13}C-NMR spectrum of the ligand $\mathbf{L_1}$ in DMSO-d_6 solvent is shown in S2. The spectrum of the ligand, S2, exhibits a chemical shift at 18.53 ppm, which is assigned

to the carbon atom of the methyl group, which is attached to the azomethine group (-N=C-**C**H_3). It was reported that the chemical shifts of the carbon atom in the methyl group of C-**C**H_3 in the range 19.09–19.87 [22]. The chemical shift at 21.3 ppm is attributed to the carbon atom of the methyl group, which is attached to the carbonyl group (-(CO)-**C**H_3). It was reported that the carbon atom of the methyl group displayed chemical shifts at 21.06 and 21.4 ppm [27]. The signals appeared in the range 40.0–32.9 ppm concerning the DMSO solvent. The chemical shift at 55.8 ppm is assigned to the carbon atom of the O-**C**H_3 group. This assignment is based on the previously reported chemical shifts of the carbon atom of this group [21-22]. The chemical shift at 59.9 ppm is due to the carbon atom of the **C**H_2 group. The reported values of the carbon atom of the CH_2 group of the mono- and diphenyl tin(IV) complexes were 59.9–60.46 ppm [28]. The chemical shift of the carbon atoms of the aromatic ring appeared in the range of 105.6–135.8 ppm [26]. The carbons of the pyrimidine ring showed three signals at 152.7, 154.3, and 161.6 ppm [26]. The peak that appeared at 162.3 ppm can be assigned to the carbon atom of the azomethine group (-**C**=N). In a previous work reported by Saheb et al., the carbon atom of the azomethine group showed a chemical shift at 162.79 ppm [21]. The signal appeared at 172.5 ppm concerning the carbon atom of the carbonyl group. The carbon atom of the carbonyl group showed chemical shifts in the reported value of 167.3–170.0 ppm [22].

Vibration Frequencies Results

Table 2 displays the selective vibrational frequencies of infrared spectra of the synthesized complexes and ligands. The assignments for the observed infrared bands were made primarily based on the vibration modes as calculated (theoretically) and on the literature data [27-32]. The infrared spectrum of the free ligand $\mathbf{L_1}$ exhibits a sharp band at 1658 cm^{-1}, which is assigned to ν(−C=N−). This vibrational band appears at a lower frequency, in the range 1642–1645 cm^{-1}, in the infrared spectra of all complexes. The shifting of the ν(−C=N−) to the lower frequency after complexation indicates coordination with the metal ion through the nitrogen atom of the −C=N− group. The vibrational frequency of the $\mathbf{L_1}$ ligand at 1682 cm^{-1}, which is assigned to the ν(C=O) of the acetyl group, is shifted to lower frequencies in the infrared spectra of complexes **1**, **2**, and **3** and appears in the range of 1670−1674 cm^{-1} indicating the coordination is through the oxygen atom of the acetyl group of the $\mathbf{L_1}$ ligand. In the cases of complexes **4** and **5**,

Table 2. Experimental and calculated infrared absorption (cm^{-1}) data of the free ligand and complexes

Compounds	ν(C=O)[b]	ν(−C=N−)	ν(C-O)[c]	ν(M-N)	ν(M-O)[c]	ν(M-O)[b]
$\mathbf{L_1}$	1682 (1693)[a]	1658 (1665)[a]	-	-	-	-
$\mathbf{L_2}$	-	-	1277 (1310)[a]	-	-	-
1	1670 (1689)[a]	1645 (1643)[a]	1238 (1273)[a]	524 (565)[a]	480 (488)[a]	459 (443)[a]
2	1671 (1680)[a]	1643 (1651)[a]	1235 (1272)[a]	526 (536)[a]	475 (470)[a]	448 (422)[a]
3	1674 (1677)[a]	1643 (1651)[a]	1242 (1270)[a]	542 (551)[a]	484 (473)[a]	438 (401)[a]
4	1681 (1694)[a]	1642 (1638)[a]	1240 (1265)[a]	513 (553)[a]	479 (447)[a]	-
5	1680 (1694)[a]	1643 (1650)[a]	1245 (1270)[a]	532 (533)[a]	472 (463)[a]	-

[a]: Calculated value at the B3LYP level of theory with the 6-311G* basis set for C, H, O, and N atoms and LANL2DZ basis set for metal atom., ν: stretching, **M**: the corresponding metal, [b]: oxygen of the carbonyl of $\mathbf{L_1}$ ligand, [c]: Oxygen of $\mathbf{L_2}$ ligand

the ν(C=O) of the acetyl group appeared at 1681 and 1680 cm^{-1}, respectively. These peaks are similar to that of the free ligand $\mathbf{L_1}$, indicating that the acetyl group in $\mathbf{L_1}$ does not participate in the coordination with the metal in complexes **4** and **5**. It is interesting to note that the frequency of the ν(C-O) band of the free $\mathbf{L_2}$ ligand appears at 1277 cm^{-1}, while in the infrared spectra of complexes **1**, **2**, **3**, **4**, and **5**, this band is downshifted and located at 1238, 1235, 1242, 1240, and 1245 cm^{-1}, respectively. This result suggested the coordination of the oxygen atoms of the hydroxyl group, the $\mathbf{L_2}$ ligand, with the metal ion. The downshifting of the frequency values of the ν(−C=N−), ν(C=O), and ν(C-O) bands of the complexes as compared to the free ligands are further supported by the calculated vibrational frequencies (Table 2). In the lower frequencies region of the infrared spectra of all complexes, new bands observed in the range 513–542 cm^{-1} and 472–480 cm^{-1} were ascribed to the ν(M-N) and ν(M–O) vibrations, respectively. Also, in the infrared spectra of complexes **1**, **2**, and **3**, another new band was observed at 459, 448, and 438 cm^{-1}, respectively, and assigned to the ν(M-O). Accordingly, the primary ligand $\mathbf{L_1}$ binds to the metal ion in a tridentate fashion through two nitrogen atoms and one oxygen atom in complexes **1**, **2**, and **3** and as a bidentate ligand fashion through two nitrogen atoms in the case of complexes **4** and **5** (Fig. 1). In the case of the $\mathbf{L_2}$ ligand, it binds the metal ion as bidentate donors via an oxygen atom in all complexes.

Geometry Optimization

The optimized geometry around the central metal ion in complex **1** is trigonal bipyramid, where **2** and **3** adopted a distorted square pyramid configuration. These results are based on the observation obtained from the calculated geometries according to the B3LYP level of the theory of these complexes (Fig. 2, Table 3). The distorted square pyramid of the optimized geometry around the metal ion in these complexes is due to the tension in N6-M-N8 and N8-M-O46 angles. Accordingly, we can deduce that the Schiff base ligand ($\mathbf{L_1}$) binds to the metal ion as tridentate fashion (NNO) donors, Fig. 2, and as bidentate ligand fashion (NN) donors, Fig. 3, while the (oxalate anion) binds to the metal ion as bidentate donors through oxygen atoms. The optimized geometries for complexes **4** and **5** (Fig. 3, Table 4) showed a slight N6-M-N8 angle and indicated a distorted square planar geometry.

Table 3. Selected bond angles (°) and bond distances (Å) of the optimized structures of **1**, **2**, and **3** at the B3LYP level of theory with the 6-311G* basis set for C, H, O, and N atoms and LANL2DZ basis set for metal atom

Bond lengths (Å) of complex **1**		Bond lengths (Å) of complex **2**		Bond lengths (Å) of complex **3**	
Co(52)-O(46)	1.927	Cr(58)-O(46)	1.968	O(46)-Zn(58)	2.196
Co(52)-N(8)	1.926	Cr(58)-O(52)	1.921	N(6)-Zn(58)	2.125
Co(52)-N(6)	1.910	Cr(58)-O(53)	1.940	N(8)-Zn(58)	2.275
O(54)-Co(52)	1.849	N(6)-Cr(58)	2.071	Zn(58)-O(52)	1.949
O(53)-Co(52)	1.836	N(8)-Cr(58)	2.067	Zn(58)-O(53)	2.005
Angles (°) of complex **1**		Angles (°) of complex **2**		Angles (°) of complex **3**	
N(6)-Co(52)-N(8)	69.3	O(52)-Cr(58)-O(46)	101.9	O(52)-Zn(58)-N(6)	138.9
N(6)-Co(52)-O(46)	159.8	O(52)-Cr(58)-N(6)	131.3	O(52)-Zn(58)-O(46)	94.8
N(6)-Co(52)-O(54)	99.4	O(52)-Cr(58)-N(8)	98.9	O(52)-Zn(58)-N(8)	114.6
N(6)-Co(52)-O(53)	99.7	O(52)-Cr(58)-O(53)	83.6	O(52)-Zn(58)-O(53)	85.8
N(8)-Co(52)-O(46)	93.0	O(46)-Cr(58)-N(6)	116.8	N(6)-Zn(58)-O(46)	120.2
N(8)-Co(52)-O(54)	168.7	O(46)-Cr(58)-N(8)	79.1	N(6)-Zn(58)-N(8)	60.3
N(8)-Co(52)-O(53)	93.6	O(46)-Cr(58)-O(53)	132.6	N(6)-Zn(58)-O(53)	89.3
O(46)-Co(52)-O(54)	98.2	N(6)-Cr(58)-N(8)	63.5	O(46)-Zn(58)-N(8)	76.4
O(46)-Co(52)-O(53)	90.8	N(6)-Cr(58)-O(53)	90.2	O(46)-Zn(58)-O(53)	126.5
O(54)-Co(52)-O(53)	87.9	N(8)-Cr(58)-O(53)	147.2	N(8)-Zn(58)-O(53)	149.5

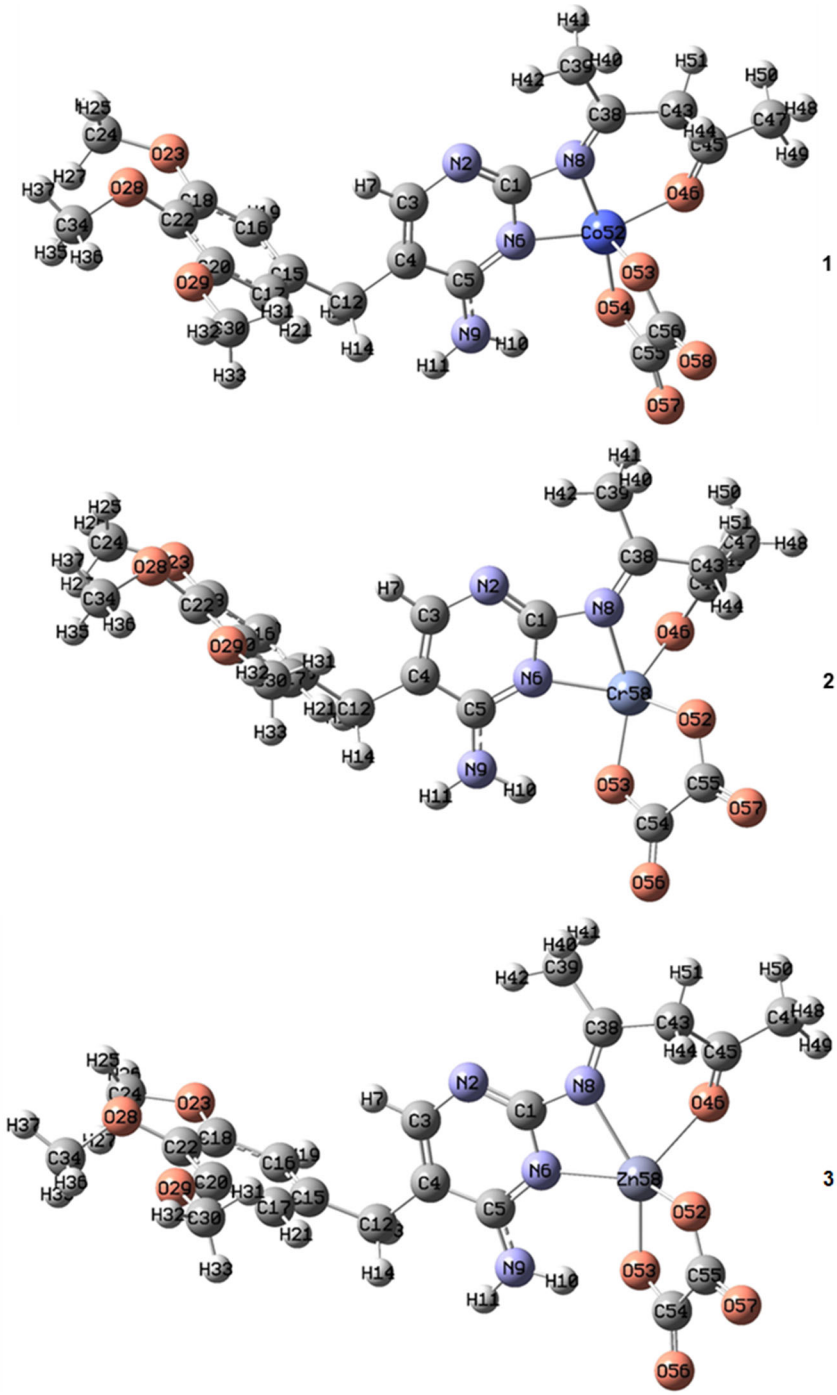

Fig 2. The optimized structures of **1**, **2,** and **3** complexes at the B3LYP level of theory with the 6-311G* basis set for C, H, O, and N atoms and LANL2DZ basis set for metal atom

The μ_{eff} value for complex **1** is 4.86, complex **2** is 3.52, and complex **4** is 1.98 BM, respectively, while the μ_{eff} values for complex **3** and **5** are approximately zero (diamagnetic).

The electronic spectral studies of compounds were carried out in DMSO (10^{-3} M) solution [33-36]. Oxalic acid in the DMSO solvent showed two high intensive bands at 262 nm (38167 cm^{-1}) attributed to $\pi \rightarrow \pi^*$ and at 310 nm (28490 cm^{-1}) attributed to $n \rightarrow \pi^*$, respectively. The spectrum of the free ligand ($\mathbf{L_1}$) showed a strong band

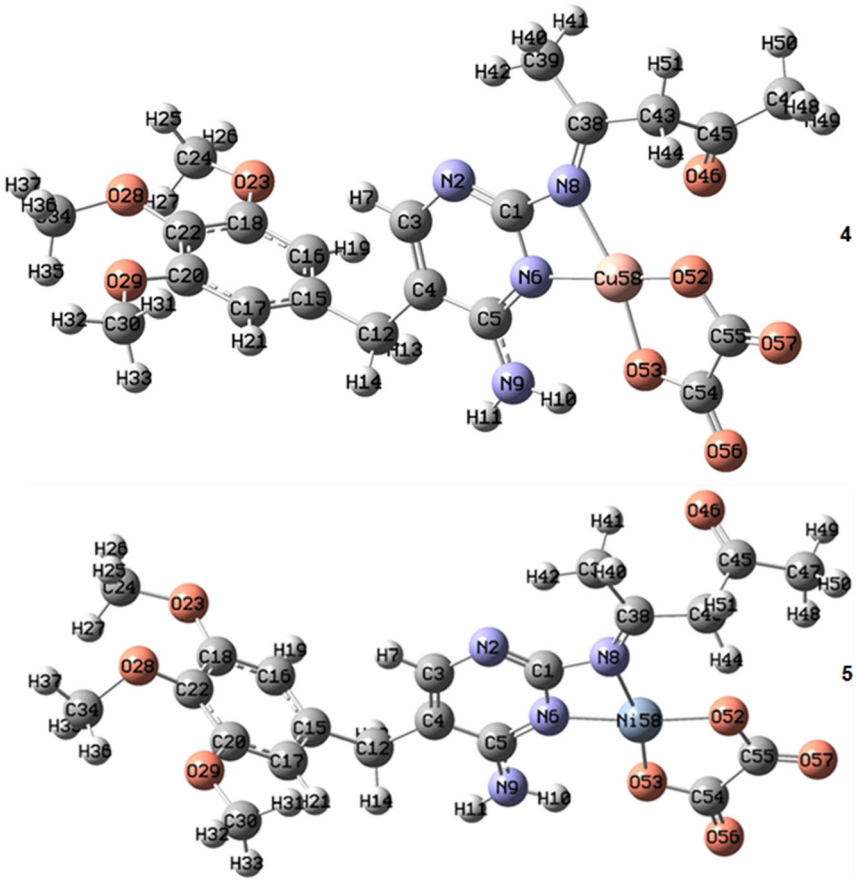

Fig 3. The optimized structures of **4** and **5** complexes at the B3LYP level of theory with the 6-311G* basis set for C, H, O, and N atoms and LANL2DZ basis set for metal atom

Table 4. Selected bond angles and bond distances (Å) of the optimized structure of **4** and **5** at the B3LYP level of theory with the 6-311G* basis set for C, H, O, and N atoms and LANL2DZ basis set for metal atom

Bond lengths (Å) of complex **4**		Bond lengths (Å) of complex **5**	
Cu(58)-O(52)	1.877	Ni(58)-O(52)	1.844
Cu(58)-N(8)	2.026	Ni(58)-N(8)	1.987
Cu(58)-O(53)	1.876	Ni(58)-O(53)	1.846
Cu(58)-N(6)	1.949	Ni(58)-N(6)	1.886
Angles (°) of complex **4**		Angles (°) of complex **5**	
N(6)-Cu(58)-N(8)	67.0	N(6)-Ni(58)-N(8)	68.5
N(6)-Cu(58)-O(52)	168.3	N(6)-Ni(58)-O(52)	173.8
N(6)-Cu(58)-O(53)	98.6	N(6)-Ni(58)-O(53)	97.7
N(8)-Cu(58)-O(52)	107.6	N(8)-Ni(58)-O(52)	105.4
N(8)-Cu(58)-O(53)	165.6	N(8)-Ni(58)-O(53)	166.2
O(52)-Cu(58)-O(53)	86.3	O(52)-Ni(58)-O(53)	88.3

at 281 nm (35587 cm^{-1}), which may be ascribed to $\pi \rightarrow \pi^*$ electronic transition within the organic ligand.

Complex **1** is considered distorted trigonal bipyramidal, and the electronic spectrum might be assigned in the "regular" geometry. In a trigonal-bipyramidal ligand field, the ground term is split into the states $^4A_2'$, $^4A_1''$, $^4A_2''$, $^4E''$, and $^4E'$; the ^4P term is split into $^4A_2'$ and $^4E''$. The electronic spectrum of complex **1** (d^7,

Term symbol of ^4F) exhibits four bands, the first band at 279 nm (35842 cm^{-1}) assigned to the charge transfer transition. The other three bands are due to d-d transitions at 526 nm (19011 cm^{-1}) ,672 nm (14880 cm^{-1}), and 826 nm (12106 cm^{-1}), which are assigned to $^4A_2'(F)\rightarrow{}^4A1''(F)$, $^4A_2'(F)\rightarrow{}^4A_2''(F)$, $^4A_2'(F)\rightarrow{}^4E''(F)$ transitions, respectively [36-40].

The electronic spectral data of the chromium complex (complex **2**) reveal four bands at 604 nm (16556 cm^{-1}), 509 nm (19646 cm^{-1}), 425 nm (23529 cm^{-1}), and 277 nm (36101 cm^{-1}), (Table 3 and 4) [29-30]. The intense high band appearing at 277 nm is assigned to the $\pi\rightarrow\pi^*$ transition of the benzene ring. Furthermore, the band at 425 nm is assigned to the $n\rightarrow\pi^*$ transitions of the azomethine group. The electronic spectrum of the Cr(III) complex showed two bands at 509 and 604 nm. The spectral band is consistent with that of five coordinated Cr(III) complexes (Cr(III), d^3, Term symbol of ^4F), so a "regular" square-pyramidal geometry may be assigned for this complex [34-35,41]. However, distorted geometry is observed in this instance. The zinc(II) complex (complex **3**) displays multiple intense absorption bands in the UV region at 281 nm (35587cm^{-1}) that we assume result from metal-ligand charge-transfer and ligand internal transitions, which is compatible with this complex having distorted square pyramid structures [35-36].

The electronic spectrum of complex **4** displays a broad single d-d band that appeared at 859 nm (11641 cm^{-1}) which implies the three allowed spin transitions, $^2B_{1g}\rightarrow{}^2A_{1g}(\nu_1)$, $^2B_1\rightarrow{}^2B_{2g}(\nu_2)$ and $^2B_1\rightarrow{}^2E_g$, may be due to square planar (slightly distorted) geometry around the copper(II) ion and 281 nm (35587 cm^{-1}) which assigned to ligand to metal charge transfer (LMCT) [37].

The (UV-Vis) spectrum of complex **5** exhibits four bands; the first band at 279 nm (35842 cm^{-1}) is assigned to the $\pi\rightarrow\pi^*$ transition of the aromatic ring. The second band appeared at 419 nm (23866 cm^{-1}), which is attributed to the charge transfer from ligand, azomethine, to metal. From the electronic spectrum, the observed peak at (628 nm) 15923 cm^{-1} is assigned to the $^1A_1\rightarrow{}^1B_1$ band and 778 nm (12853 cm^{-1}), which is attributed to the $^1A_1\rightarrow{}^1A_2$ band. These transitions suggest the square planar geometry around Ni(II). The 10 Dq = 2853 cm^{-1}, and ν_1/ν_2 = 80 (or ν_2/ν_1 = 1.23 are in the usual range reported for a distorted square planar of the Ni(II) complexes [38].

Electronic Structures

The calculated electron densities and energies of the frontiers' molecular orbitals (HOMO and LUMO) were investigated to explain the electronic properties of the prepared complexes. Fig. 4 and 5 summarize the calculated absolute energies of the HOMO and LUMO orbitals together with the HOMO-LUMO energy gap values. Complex **5** has a more significant HOMO-LUMO energy gap. The calculated orbital energy levels and percent composition of particular chosen frontier inhabited and virtual molecular orbitals of the prepared compounds, expressed in terms of composing fragments ($\mathbf{L_1}$, $\mathbf{L_2}$, and metal ion), are listed in Table 5. As shown in Table 5, the HOMO of complex **1** is wholly localized on the $\mathbf{L_1}$ ligand, and its LUMO complex is mainly localized on the metal ion. The HOMO and LUMO of complex **2** are mainly localized on the metal ion, as shown in Fig. 4 and presented in Table 5. The percent composition of frontier occupied and virtual molecular orbitals of complex **3** differ from those of complexes **1** and **2**, as shown in Table 5. The ligands $\mathbf{L_1}$ and $\mathbf{L_2}$ of complex **3** contribute 100% of LUMO and 99% of HOMO, respectively. The LUMO orbital of complex **4** is distributed over metal ions, $\mathbf{L_1}$ and $\mathbf{L_2}$, with almost equal percent, while its HOMO orbital is almost localized on the metal ion (Fig. 5, Table 5). The percent composition of HOMO and LUMO molecular orbitals of complex **5** are very similar to those of complex **3** (Fig. 5, Table 5).

Molecular Electrostatic Potential

The generated molecular electrostatic potential in the space around a molecule, including the charge distribution, is very helpful in understanding the sites for electrophilic attacks and nucleophilic reactions. Also, exploring the charge distribution around the molecule is essential for studying biological recognition processes and hydrogen bonding interactions [42-45]. Hence, the molecular electrostatic potentials for complexes **2** and **5** were calculated from the optimized geometry (Fig. 6). The

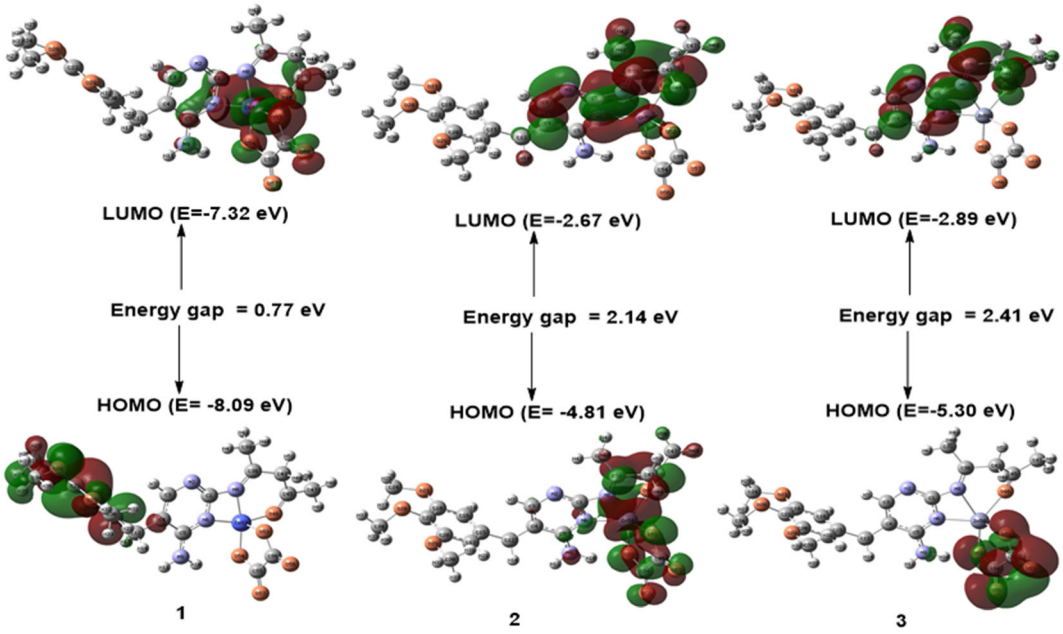

Fig 4. The frontier orbitals, HOMO, and LUMO of the complexes **1**, **2**, and **3** were calculated at the B3LYP level of theory with the 6-311G* basis set for C, H, O, and N atoms and LANL2DZ basis set for metal atom, with the surface isovalue of 0.02

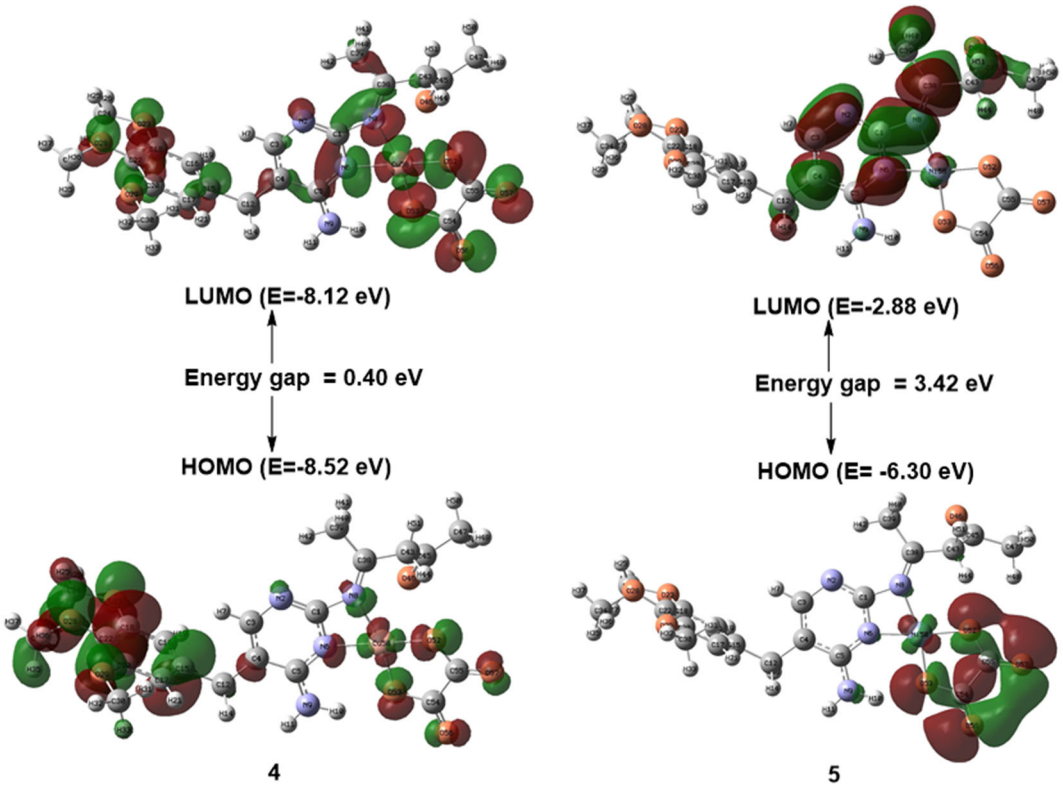

Fig 5. The frontier orbitals, HOMO, and LUMO of complexes **4** and **5** were calculated at the B3LYP level of theory with the 6-311G* basis set for C, H, O, and N atoms and LANL2DZ basis set for metal atoms, with the surface isovalue is 0.02

Table 5. Energies and percent composition of HOMO and LUMO molecular orbitals of complexes, expressed in terms of composing fragments, calculated at the B3LYP level of theory with the 6-311G* basis set for C, H, O, and N atoms and LANL2DZ basis set for metal atom

Compound	Molecular orbital	Orbital energy (eV)	Fragment		
			Metal	L_1 ligand	L_2 ligand
1	LUMO	-7.32	62	12	26
	HOMO	-8.09	0	100	0
2	LUMO	-2.67	63	17	20
	HOMO	-4.81	83	8	9
3	LUMO	-2.89	0	100	0
	HOMO	-5.30	0	1	99
4	LUMO	-8.12	30	31	39
	HOMO	-8.52	5	88	7
5	LUMO	-2.88	1	99	0
	HOMO	-6.30	3	1	96

electrophilic reactive sites of the molecule are concerned with the negative (red) regions of molecular electrostatic potential (Fig. 6). The nucleophilic reactive sites are regarded by the positive (blue) regions of molecular electrostatic potential. For complex **2**, the negative electrostatic potential regions are mainly localized over the O57, O56, O23, O28, and N2 atoms (Fig. 6). The V(r) values are -0.092, -0.085, -0.032, -0.037 and -0.022 a.u. for O57, O56, O23, O28 and N2 atoms of complex **2**, respectively. According to these results, complex **2** has five possible sites for the electrophilic attack. The most positive electrostatic potential is localized on the C47–H50 (V(r) = 0.045 a.u.) region of complex **2**. Therefore, the C47–H50 region represents the most reactive site toward nucleophilic attack within complex **2**. For complexes **1** and **3**, the most positive and negative electrostatic potentials are similar to those observed for complex **2**. For the complex **5**, the negative electrostatic potential regions are mainly localized over the O57 (V(r) = -0.080 a.u.), O56 (V(r) = -0.079 a.u.), O46 (V(r) = -0.028 a.u.), and O29 (V(r) = -0.036 a.u.) atoms (Fig. 6). Accordingly, the O57, O56, O46, and O29 atoms represent the possible sites for the electrophilic attack of the complex **5**. The most positive electrostatic potential region is localized on the N9–H11 (V(r) = 0.049 a.u.) of the complex **5**. Therefore, the region N9–H11, in complex **5**, is an electrophilic site and represents the most reactive site toward nucleophilic attack. For complex **4** the most positive and negative electrostatic potentials are similar to those observed for complex **5**.

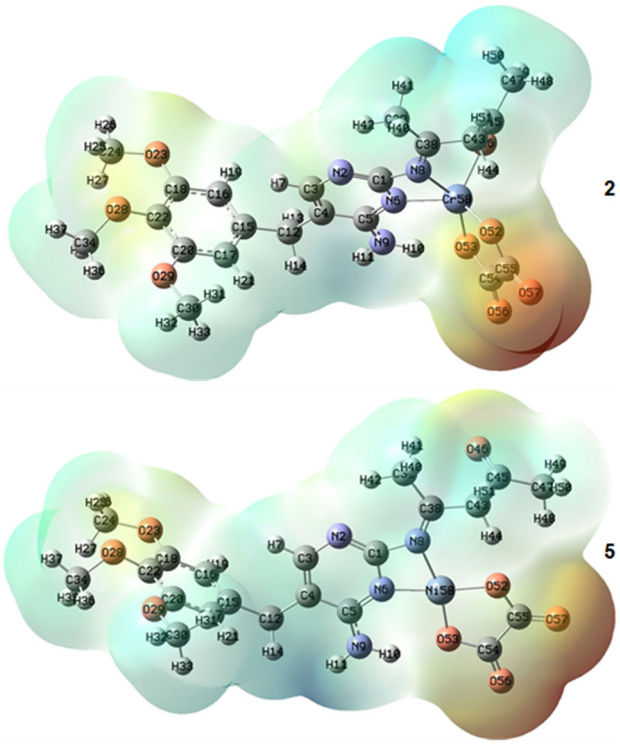

Fig 6. The Molecular electrostatic potential map of complexes **2** and **5**

Antibacterial Activities

The comparative study of the biological effects of the ligands and their complexes is listed in Fig. 7. The synthesized complexes have been tested against the

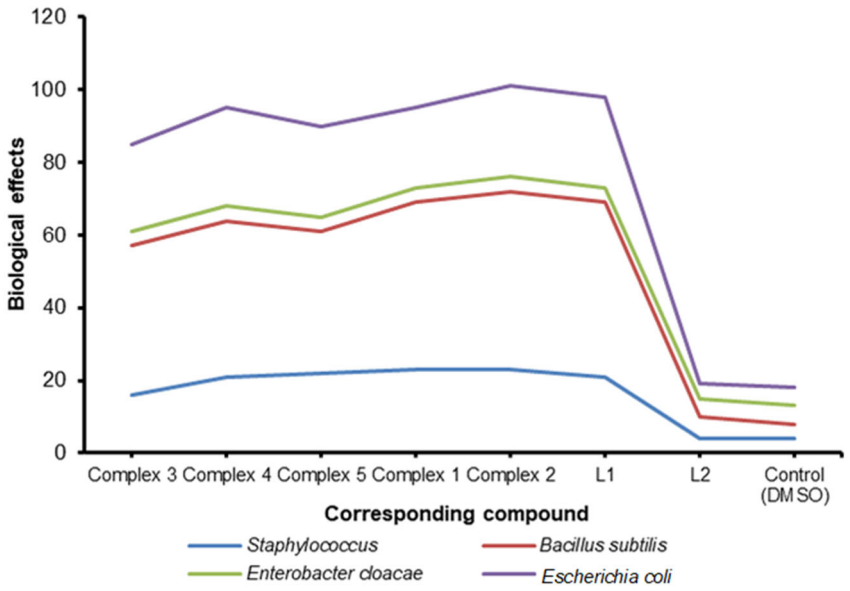

Fig 7. The biological effect of compounds

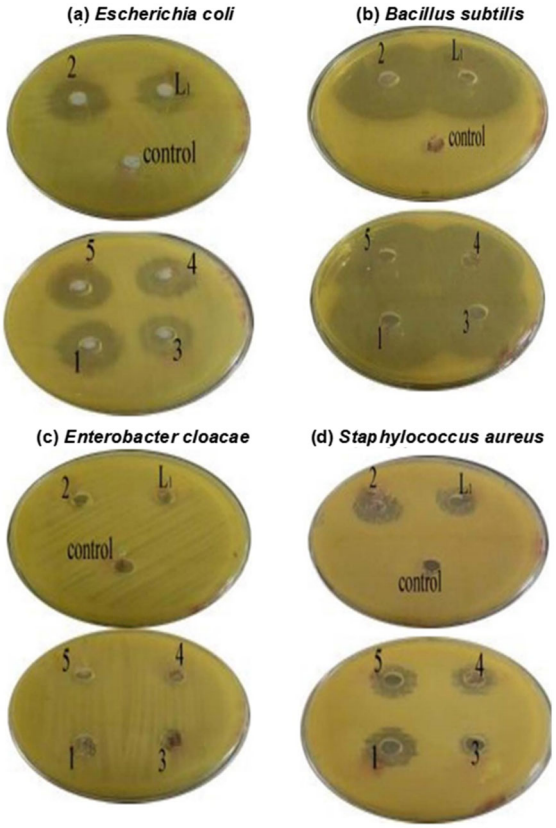

Fig 8. Photograph of the zone of inhibition in mm antibacterial activity of compounds

growth of *Escherichia coli*, *Enterobacter cloacae*, *Staphylococcus aureus*, and *Bacillus subtilis*. Generally, the antibacterial activities were in the order: Complex **2** > $\mathbf{L_1}$ > complex **5** > complex **4** ≈ complex **1** > complex **3** > $\mathbf{L_2}$ = DMSO. This finding means that complexes significantly affect the antimicrobial activity of the organic ligand. Fig. 8. The antibacterial activity (ZI) of all the complexes >> Oxalic acid ≈ DMSO. The DMSO was used as a solvent and negative control. It did not show any activity against bacteria. All tests lacked antibacterial activity against *Enterobacter cloacae*. All complex tests had anti-bacterial activity against test bacteria (*Escherichia coli*, *Staphylococcus aureus*, and *Bacillus subtilis*). The results showed that the nature of the metal ion (M(II), Cr(III)) in complexes plays a significant role in the ZI activity [46]. Also, the structure of $\mathbf{L_1}$ due to the presence of the (C=N) group, which is significant in the mechanism reactions in biological reactions, and ligands with (N) and (O) donor systems might inhibit enzyme production and possibly (π-e) delocalization through the whole (chelate ring) system thus include through coordination [46].

DNA Binding Properties

The electrophoresis diagram of compounds is in Fig. 9. In comparison to control samples 1 and 2, there was a complete breakage in samples 3 and 10, which represented CrA and DMSOA, respectively, and the number 5 (lane 5), which represented NiA, was not found to be broken, and in samples 4 (lane 4), 6 (lane 6),

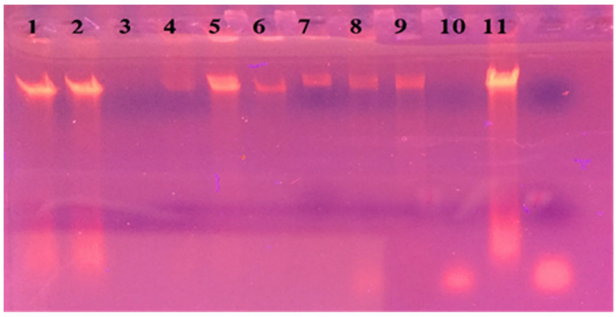

1: control; 2: control; 3: CrA; 4: OxA; 5: NiA; 6: CuA; 7: ZnA; 8: DNA control; 9: TMA; 10: DMSOA; 11: control

Fig 9. Agarose gel electrophoresis pattern for the DNA binding studies of oxalic acid and Schiff base trimethoprim with various metal ions

7 (lane 7), 8 (lane 8), and 9 (lane 9), representing OxA, CuA, ZnA, DNA control 3, and TMA, respectively. The most influential sample on DNA was sample 8 (lane 8), which represents DNA control, where a long haze streak showed DNA breaking along the gel transfer line. In the DNA cracking that was detected by the weak radiation of the sample and the use of Red safe stain at the examination under the source of ultraviolet compared to the control sample. The intensity of the metal-DNA bands is also reduced when compared to the DNA control [39,46].

■ CONCLUSION

The new mixed ligand complexes are synthesized from the reaction of Schiff base ligand, $\mathbf{L_1}$, and oxalate anion, $\mathbf{L_2}$, with metal salts. The synthesized Schiff base ligand, $\mathbf{L_1}$, was prepared from the reaction of trimethoprim and acetylacetone. The general formula of the synthesized complexes is $[\mathbf{M}(\mathbf{L_1})(\mathbf{L_2})]$, where **M** represents one of the following metals Co(II), Ni(II), Cu(II), Zn(II), and Cr(III), $\mathbf{L_1}$ represents the trimethoprim ((*Z*)-4-((4-amino-5-(3,4,5-trimethoxybenzyl)pyrimidine-2-yl)imino)pentane-2-one) as the first ligand and $\mathbf{L_2}$ represent the oxalate anion ($C_2O_2^{2-}$) as a second ligand. The analytical and conductivity measurements support the proposed formulae and indicate that the complexes are non-electrolytes except complex **2**, which is a 1:1 electrolyte. The results obtained from measurements of UV, IR, and NMR are in good agreement with the optimized structures of these complexes, which are calculated at the B3LYP level of theory with the 6-311G* basis set for C, H, O, and N atoms and LANL2DZ basis set for metal atom. The Schiff base, $\mathbf{L_1}$, coordinated to the metal ion in a tridentate fashion through two nitrogen atoms and one oxygen atom in the case of complexes **1**, **2**, and **3**, which adopted highly distorted trigonal bipyramid for complex **1**, and distorted square pyramid configuration for **2** and **3**, and as bidentate ligand fashion through two nitrogen atoms in the case of complexes **4** and **5** which adopted a highly distorted square planar geometry. The molecular electrostatic potential of the complexes is explored. The results show that the negative electrostatic potential regions are mainly localized over the oxygen atoms in most cases. The electronic structures of the complexes are investigated in terms of the energies of the HOMO and LUMO orbitals and the electron density distribution of these orbitals over the composing fragments ($\mathbf{L_1}$, $\mathbf{L_2}$, and metal ions) of the complexes. The antibacterial activities of the prepared compounds were in the order: complex **2** > $\mathbf{L_1}$ > complex **5** > complex **4** ≈ complex **1** > complex **3** >$\mathbf{L_2}$. In the DNA cracking that was detected by the weak radiation of the sample and the use of a Red safe stain, it is observed that the intensity decreased for the metal-DNA bands compared to DNA control.

■ ACKNOWLEDGMENTS

The authors wish to thank the technical assistance provided by the Departments of Chemistry in Baghdad and Al-Mustansiriya university in the preparation of the samples for antimicrobial activities are also acknowledged.

■ AUTHOR CONTRIBUTIONS

All authors contributed to the study's conception and design. Material preparation, data collection, and analysis were performed by Eid Abdalrazaq, Abdel Aziz Qasem Jbarah, Tagreed H. Al-Noor, G.T. Shinain, and M.M. Jawad. Tagreed H. Al-Noor wrote the first draft of the manuscript, and all authors commented on previous versions. All authors read and approved the final manuscript.

■ REFERENCES

[1] El-Sawaf, A.K., El-Essawy, F., Nassar, A.A., and El-Samanody, E.S.A., 2018, Synthesis, spectral, thermal and antimicrobial studies on cobalt(II), nickel(II), copper(II), zinc(II) and palladium(II) complexes containing thiosemicarbazone ligand, *J. Mol. Struct.*, 1157, 381–394.

[2] Muralisankar, M., Haribabu, J., Bhuvanesh, N.S.P., Karvembu, R., and Sreekanth, A., 2016, Synthesis, X-ray crystal structure, DNA/protein binding, DNA cleavage and cytotoxicity studies of *N*(4) substituted thiosemicarbazone based copper(II)/nickel(II) complexes, *Inorg. Chim. Acta*, 449, 82–95.

[3] Mathan Kumar, S., Rajesh, J., Anitha, K., Dhahagani, K., Marappan, M., Indra Gandhi, N., and Rajagopal, G., 2015, Synthesis, characterization, crystal structure and cytotoxic properties of thiosemicarbazide Ni(II) and Zn(II) complexes, *Spectrochim. Acta, Part A*, 142, 292–302.

[4] Pahonţu, E., Julea, F., Chumakov, Y., Petrenco, P., Roşu, T., and Gulea, A., 2017, Synthesis, characterization, crystal structure and antiproliferative activity studies of Cu(II), Ni(II) and Co(II) complexes with 4-benzoyl-5-pyrazolones derived compounds, *J. Organomet. Chem.*, 836-837, 44–55.

[5] Pu, L.M., Zhao, Q., Liu, L.Z., Zhang, H., Long, H.T., and Dong, W.K., 2018, Synthesis and fluorescence properties of a new heterotrinuclear Co(II)-Ce(III)complex constructed from a bis(salamo)-type tetraoxime ligand, *Molecules*, 23 (4), 804.

[6] Chen, Q.L., 2016, Synthesis and structural characterization of a pyridine oxalato molybdenum(V) complex, *Int. J. New Technol. Res.*, 2 (1), 40–43.

[7] Frisch, M.J., Trucks, G.W., Schlegel, H.B., Scuseria, G.E., Robb, M.A., Cheeseman, J.R., Scalmani, G., Barone, V., Mennucci, B., Petersson, G.A., Nakatsuji, H., Caricato, M., Li, X., Hratchian, H.P., Izmaylov, A.F., Bloino, J., Zheng, G., Sonnenberg, J.L., Hada, M., Ehara, M., Toyota, K., Fukuda, R., Hasegawa, J., Ishida, M., Nakajima, T., Honda, Y., Kitao, O., Nakai, H., Vreven, T., Montgomery, J.A., Jr., Peralta, J.E., Ogliaro, F., Bearpark, M., Heyd, J.J., Brothers, E., Kudin, K.N., Staroverov, V.N., Kobayashi, R., Normand, J., Raghavachari, K., Rendell, A., Burant, J.C., Iyengar, S.S., Tomasi, J., Cossi, M., Rega, N., Millam, J.M., Klene, M., Knox, J.E., Cross, J.B., Bakken, V., Adamo, C., Jaramillo, J., Gomperts, R., Stratmann, R.E., Yazyev, O., Austin, A.J., Cammi, R., Pomelli, C., Ochterski, J.W., Martin, R.L., Morokuma, K., Zakrzewski, V.G., Voth, G.A., Salvador, P., Dannenberg, J.J., Dapprich, S., Daniels, A.D., Farkas, Ö., Foresman, J.B., Ortiz, J.V., Cioslowski, J., and Fox, D.J., 2009, *Gaussian-09 Revision E.01*, Gaussian, Inc., Wallingford, CT.

[8] Makkonen, I., Ervasti, M.M., Kauppila, V.J., and Harju, A., 2012, Exchange-correlation potentials for inhomogeneous electron systems in two dimensions from exact diagonalization: Comparison with the local-spin-density approximation, *Phys. Rev. B*, 85, 205140.

[9] Becke, A.D., 2019, Dependence of the virial exciton model on basis set and exact-exchange fraction, *J. Chem. Phys.*, 150, 241101.

[10] Chen, H., Nusspickel, M., Tilly, J., and Booth, G.H., 2021, Variational quantum eigensolver for dynamic correlation functions, *Phys. Rev. A*, 104 (3), 032405.

[11] Wang, G., Annaberdiyev, A., Melton, C.A., Bennett, M.C., Shulenburger, L., and Mitas, L., 2019, A new generation of effective core potentials from correlated calculations: 4s and 4p Main group elements and first row additions, *J. Chem. Phys.*, 151, 144110.

[12] Hill, J.G., and Shaw, R.A., 2021, Correlation consistent basis sets for explicitly correlated wavefunctions: Pseudopotential-based basis sets for the group 11 (Cu, Ag, Au) and 12 (Zn, Cd, Hg) elements, *J. Chem. Phys.*, 155, 174113.

[13] Hassan, S.S., Shoukry, M.M., and Jbarah, A.A.Q., 2020, Cordination compound of dimethyltin(IV) with *N*,*N*,*N*',*N*'-tetraethylethylenediamine: speciation and theoretical approach, *J. Mex. Chem. Soc.*, 64 (2), 24–43.

[14] Dennington, R., Keith, T.A., and Millam, J.M., 2016, *GaussView, Version 6*, Semichem Inc., Shawnee Mission, KS.

[15] Abu-Yamin, A.A., Jbarah, A.A.Q.M., AlKhalyfeh, K., Matar, S., Alqasaimeh, M., Rüffer, T., and Lang,

H., 2022, Crystal structure, spectroscopic studies, DFT calculations, and biological activity of 5-bromosalicylaldehyde–based Schiff bases, *J. Mol. Struct.*, 1262, 132976.

[16] O'boyle, N.M., Tenderholt, A.L., and Langner, K.M., 2008, Cclib: A library for package-independent computational chemistry algorithms, *J. Comput. Chem.*, 29 (5), 839–845.

[17] Mary Juliet, B.M., and Amaladasan, M., 2014, Preparation and properties of macrocyclic ligand, *Int. J. Recent Innovation Trends Comput. Commun.*, 2 (8), 2102–2105.

[18] Jeffery, G.H., Bassett, J., Mendham, J., and Denney, R.C., 1989, *Vogel's Textbook of Quantitative Chemical Analysis*, 5th Ed., John Wiley & Sons Inc., New York, US.

[19] Orekhov, M.A., 2021, Coordination numbers of bivalent ions in organic solvents, *Russ. J. Phys. Chem. A*, 95 (10), 2059–2064.

[20] Marcus, R.A., 1964, Chemical and electrochemical electron-transfer theory, *Annu. Rev. Phys. Chem.*, 15 (1), 155–196.

[21] Saheb, V., Sheikhshoaie, I., and Stoeckli-Evans, H., 2012, A novel tridentate Schiff base dioxo-molybdenum(VI) complex: Synthesis, experimental and theoretical studies on its crystal structure, FTIR, UV–visible, ^{1}H NMR and ^{13}C NMR spectra, *Spectrochim. Acta, Part A*, 95, 29–36.

[22] Agrwal, A., Verma, A., Chantola, N., Verma, S., and Kasana, V., 2022, Synthesis, molecular docking and extensive structure activity relationship of substituted DHP derivatives: A new class of herbicides, *J. Environ. Sci. Health, Part B*, 57 (5), 379–420.

[23] Odion, E.E., Enadeghe, D.O., and Usifoh, C.O., 2021, Synthesis, characterization and antibacterial assessment of 3,4,5-trimethoxy-3',4'-dimethoxychal cone and 2,4,6-trimethoxy-3',4'-dimethoxychalcone, *Niger. J. Pharm. Appl. Sci. Res.*, 10 (2), 1–5.

[24] Jin, R.Y., Sun, X.H., Liu, Y.F., Wong, W., Lu, W.T., and Ma, H.X., 2014, Synthesis, crystal structure, IR, ^{1}H NMR and theoretical calculations of 1,2,4-triazole Schiff base, *J. Mol. Struct.*, 1062, 13–20.

[25] Aparna, E.P., and Devaky, K.S., 2018, Microwave assisted solid phase synthesis of trisubstituted pyrimidines, *J. Chem. Pharm. Res.*, 10 (8), 67–72.

[26] Jacobsen, N.E., 2017, *NMR Data Interpretation Explained: Understanding 1D and 2D NMR Spectra of Organic Compounds and Natural Products*, John Wiley & Sons, Inc., Hoboken, New Jersey, US.

[27] Ebrahimi, H.P., Hadi, J.S., Abdulnabi, Z.A., and Bolandnazar, Z., 2014, Spectroscopic, thermal analysis and DFT computational studies of salen-type Schiff base complexes, *Spectrochim. Acta, Part A*, 117, 485–492.

[28] Adeyemi, J.O., Olasunkanmi, L.O., Fadaka, A.O., Sibuyi, N.R.S., Oyedeji, A.O., and Onwudiwe, D.C., 2022, Synthesis, theoretical calculation, and biological studies of mono- and diphenyltin(IV) complexes of *N*-methyl-*N*-hydroxyethyldithio carbamate, *Molecules*, 27 (9), 2947.

[29] Al-Noor, T.H., Karam, N.H., Ghanim, F.H., Kindeel, A.S., and Al-Dujaili, A.H., 2017, Synthesis, characterization and liquid crystalline properties of novel benzimidazol-8-hydroxyquinoline complexes, *Inorg. Chim. Acta*, 466, 612–617.

[30] Nakamoto, K., 2009, *Infrared and Raman Spectra of Inorganic and Coordination Compounds, Part B: Applications in Coordination, Organometallic, and Bioinorganic Chemistry*, 6th Ed., John Wiley & Sons, Inc., Hoboken, New Jersey, US.

[31] Mezey, R.Ș., Máthé, I., Shova, S., Grecu, M.N., and Roșu, T., 2015, Synthesis, characterization and antimicrobial activity of copper(II) complexes with hydrazone derived from 3-hydroxy-5-(hydroxymethyl)-2-methylpyridine-4-carbaldehyde, *Polyhedron*, 102, 684–692.

[32] Bellamy, L.J., 1975, *The Infra-Red Spectra of Complex Molecules*, Springer, Dordrecht, Netherlands.

[33] Housecroft, C.E., and Sharpe, A.G., 2018, *Inorganic Chemistry*, 5th Ed., Pearson Education Limited, Harlow, UK.

[34] Jamil, Y.M.S., Al-Qadasy, J.M.K., Al-Azab, F.M., and Al-Maqtari, M.A., 2018, Synthesis, characterization and antibacterial study of some 3d-metal complexes

of paracetamol and 1,10-phenanthroline, *Jordan J. Chem.*, 13 (4), 203–212.

[35] Fleming, G.R., Lewis, N.H.C., Arsenault, E.A., Wu, E.C., and Oldemeyer, S., 2019, "Two-Dimensional Electronic Vibrational Spectroscopy" in *Coherent Multidimensional Spectroscopy*, Eds. Cho, M., Springer, Singapore, 35–49.

[36] Galić, N., Dijanošić, A., Kontrec, D., and Miljanić, S., 2012, Structural investigation of aroylhydrazones in dimethylsulphoxide/water mixtures, *Spectrochim. Acta, Part A*, 95, 347–353.

[37] Abbas, S.H., 2017, Synthesis, characterization and biological activity of some nickel(II) mixed ligands complexes of dithiocarbamate and 1,10-phenanthroline, *Eur. J. Chem.*, 8 (4), 367–370.

[38] Yallur, B.C., Krishna, P.M., and Challa, M., 2021, Bivalent Ni(II), Co(II) and Cu(II) complexes of [(*E*)-[(2-methyl-1,3-thiazol-5-yl)methylidene]amino]thio urea: Synthesis, spectral characterization, DNA and *in-vitro* anti-bacterial studies, *Heliyon*, 7 (4), e06838.

[39] Rajendran, N., Periyasamy, A., Kamatchi, N., and Solomon, V., 2020, Synthesis and efficacy of copper(II) complexes bearing *N*(4)-substituted thiosemicarbazide and diimine co-ligands on plasmid DNA and HeLa cell lines, *J. Serb. Chem. Soc.*, 85 (3), 321–334.

[40] Dance, I.G., Gerloch, M., Lewis, J., Stephens, F.S., and Lions, F., 1966, High-spin five-coordinate cobalt (II), *Nature*, 210 (5033), 298.

[41] Kafi-Ahmadi, L., and Shirmohammadzadeh, L., 2017, Synthesis of Co(II) and Cr(III) salicylidenic Schiff base complexes derived from thiourea as precursors for nano-sized Co_3O_4 and Cr_2O_3 and their catalytic, antibacterial properties, *J. Nanostruct. Chem.*, 7 (2), 179–190.

[42] Bendjeddou, A., Abbaz, T., Gouasmia, A., and Villemin, D., 2017, Determination of reactive properties of a series of mono-functionalized bis-tetrathiafulvalene employing DFT calculations, *ASRJETS*, 29 (1), 308–326.

[43] Politzer, P., and Murray, J.S., 2021, "Molecular Electrostatic Potentials: Significance and Applications" in *Chemical Reactivity in Confined Systems: Theory, Modelling and Applications*, Eds. Chattaraj, P.K., and Chakraborty, D., John Wiley & Sons Ltd, Hoboken, New Jersey, US.

[44] Gadre, S.R., Suresh, C.H., and Mohan, N., 2021, Electrostatic potential topology for probing molecular structure, bonding and reactivity, *Molecules*, 26 (11), 3289.

[45] da Silva, G.C.Q., Cardozo, T.M., Amarante, G.W., Abreu, C.R.A., and Horta, B.A.C., 2018, Solvent effects on the decarboxylation of trichloroacetic acid: Insights from *ab initio* molecular dynamics simulations, *Phys. Chem. Chem. Phys.*, 20 (34), 21988–21998.

[46] Muthukkumar, M., Malathy, M., and Rajavel, R., 2015, Antimicrobial and DNA cleavage activities of macrocyclic Cu(II), Ni(II), Co(II), and Zn(II) Schiff base complexes, *Chem. Sci. Rev. Lett.*, 4 (16), 1227–1236.